AFRL-DE-PS-
TR-2005-1095

INVESTIGATION OF BURST PRESSURES PREDICTION OF SLIT ALUMINUM CYLINDERS SUBJECTED TO LOCALIZED HEATING

C.T. Sun, et. al.

Ball Aerospace & Technologies Corp.
System Engineering Solutions
2201 Buena Vista SE, Suite 100
Albuquerque, NM 87106

May 2005

Final Report

AIR FORCE RESEARCH LABORATORY
Directed Energy Directorate
3550 Aberdeen Avenue SE
AIR FORCE MATERIEL COMMAND
KIRTLAND AIR FORCE BASE, NM 87117-5776

STINFO COPY

This report has been reviewed by the Public Affairs Office and is releasable to the National Technical Information Service (NTIS). At NTIS, it will be available to the general public, including foreign nationals.

If you change your address, wish to be removed from this mailing list, or your organization no longer employs the addressee, please notify AFRL/DELE, 3550 Aberdeen Avenue SE, Kirtland AFB, NM 87117-5776.

Do not return copies of this report unless contractual obligations or notice on a specific document requires its return.

This report has been approved for publication.

//Signed//

ROBERT ULIBARRI, DR-II, DAF
Project Officer

//Signed//

JORGE E. BERAUN, DR-IV, DAF
Chief, Laser Effects Research Branch

//Signed//

L. BRUCE SIMPSON, SES
Director, Directed Energy Directorate

REPORT DOCUMENTATION PAGE

Form Approved
OMB No. 0704-0188

1. REPORT DATE *(DD-MM-YYYY)*	**2. REPORT TYPE**	**3. DATES COVERED** *(From - To)*
27-05-2005	Final Report	1 June 04 – 27 March 05

4. TITLE AND SUBTITLE
Investigation of Burst Pressures Prediction of Slit Aluminum Cylinders Subjected to Localized Heating

5a. CONTRACT NUMBER
F29601-00-D-0010 / 0014

5b. GRANT NUMBER

5c. PROGRAM ELEMENT NUMBER
ASCA

6. AUTHOR(S)
C.T. Sun, T. Tanner, A. Deitemeyer, D. Nakaima, N. Bruno, D. Doering*, C. Tham **, R. Ulibarri**, and J.K. Chen**

5d. PROJECT NUMBER
LV

5e. TASK NUMBER
AB

5f. WORK UNIT NUMBER

7. PERFORMING ORGANIZATION NAME(S) AND ADDRESS(ES)
*Ball Aerospace & Technologies Corp.
Systems Engineering Solutions
2201 Buena Vista SE, Suite 100
Albuquerque, NM 87106

Purdue Research Foundation
610 Purdue Mall
West Lafayette, IN 47907-2040

8. PERFORMING ORGANIZATION REPORT NUMBER

9. SPONSORING / MONITORING AGENCY NAME(S) AND ADDRESS(ES)
**Air Force Research Laboratory
3550 Aberdeen Avenue SE
Kirtland AFB, NM 87117-5776

10. SPONSOR / MONITOR'S ACRONYM(S)

11. SPONSOR/MONITOR'S REPORT NUMBER(S)
AFRL-DE-PS-TR-2005-1095

12. DISTRIBUTION / AVAILABILITY STATEMENT
Approved for public release; distribution is unlimited.

13. SUPPLEMENTARY NOTES

14. ABSTRACT
Crack Tip Opening Angle (CTOA) measurements of aluminum alloy 2014-T6 (Al-2014-T6) at various temperatures and the construction of the corresponding CTOA curves were performed. The CTOA curve as the crack growth criterion was used to simulate the burst pressures in Al-2014-T6 thin-walled cylinders with a longitudinal crack of different sizes under thermal and mechanical load. The crack growth is simulated using nodal release method in the ABAQUS finite element environment to predict the burst pressure of axially cracked cylinders.

15. SUBJECT TERMS
Crack Tip Opening Angle, CTOA, Aluminum Alloy 2014-T6, Burst Pressures, Thin-Walled Cylinders, ABAQUS

16. SECURITY CLASSIFICATION OF:			**17. LIMITATION OF ABSTRACT**	**18. NUMBER OF PAGES**	**19a. NAME OF RESPONSIBLE PERSON**
					Robert Ulibarri
a. REPORT	**b. ABSTRACT**	**c. THIS PAGE**	SAR	36	**19b. TELEPHONE NUMBER** *(include area code)*
Unclassified	Unclassified	Unclassified			505-846-3282

Standard Form 298 (Rev. 8-98)
Prescribed by ANSI Std. 239.18

This page intentionally left blank.

CONTENTS

FIGURES

TABLES

This page is intentionally left blank.

1.0 INTRODUCTION

This report contains the results of the work performed under the contract, Effects Research, Modeling and Assessments , between Purdue University and Ball Aerospace and Technologies Corp.

The presentation is aimed at developing analysis and simulation methods for fracture instability of axially cracked cylinder subjected thermo-mechanical load. The material of interest is aluminum alloy 2014-T6 (Al-2014-T6). The first section deals with Crack Tip Opening Angle (CTOA) measurements of Al-2014-T6 at various temperatures and the construction of the corresponding CTOA curves to be input into ABAQUS finite element code for simulation of the burst pressure. Various types of curved fit CTOA curves were examined to evaluate the sensitivity of the CTOA curve as a crack growth to the burst pressure prediction. The second section is devoted to the simulation of the burst pressures in Al-2014-T6 thin-walled cylinders with a longitudinal crack of different sizes using the CTOA curve as the fracture criterion. An automate approach was implemented in the ABAQUS environment to perform the nodal release crack growth simulation for predicting the burst pressure of axially crack cylinders subjected localized heating and pressure. The data in this report should be validated by laboratory testing to confirm the analysis and the simulation presented.

2.0 RESULTS

2.1 MEASUREMENT OF CTOA CURVE FOR ALUMINUM 2014-T6

2.1.1 Room Temperature-Center Crack

The aluminum specimens were cut with a center crack in the **LT** direction, using a water-jet machine. The specimens had dimensions of: length 2L=350 mm, width W=88 mm, thickness B=3.18 mm. The crack size after the water jet cut was $2a_o$=23 mm. The notch of the crack was sharpened on either side of the center-crack. Following the jewelers saw cut, the dimension of the crack was close to $2a_o$ = 25 mm. All the specimens were fatigued at the rate of 8 Hz using a fatigue load of 0.5-15.5 kN. Specimens with two different fatigue crack lengths were tested. The fatigue crack obtained for the first specimen was of length 0.6 mm and for the second specimen, a fatigue length of 5.5 mm.

The fatigue-cracked specimens were loaded under position control at the rate of 0.001 mm/sec. As the crack began to grow, the loading was held constant at a certain length of crack extension and the digital image captured. The captured digital images were used to obtain the CTOA with crack extension for the specimens tested, using MATLAB. The stable crack extension for both the specimens was found to be less than 4 mm. Figure 1 shows images captured at very small crack extensions. The specimens failed after a small stable crack extension. Figure 2 shows a picture of the fractured center cracked aluminum specimen tested in Mode I loading. Figure 3 shows the fractured surface.

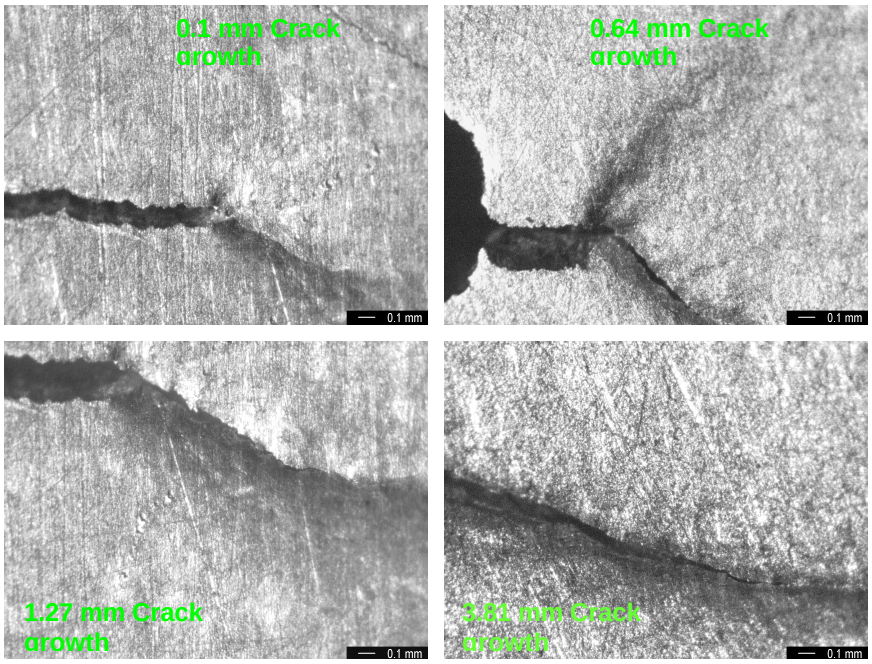

Figure 1. Crack tip region at various stages of crack growth for aluminum specimens tested at room temperature.

Figure 2. Fractured center crack specimen tested in Mode I loading.

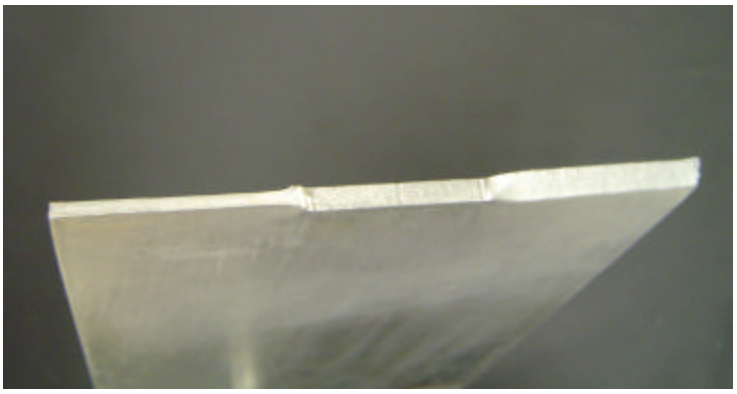

Figure 3. Fractured surface of the center crack specimen tested in Mode I loading.

2.1.2 Room Temperature-Edge Crack

The tests with center crack specimens gave very few data points for the CTOA resistance curve for aluminum (Al-2014-T6) since the length of stable crack propagation was about 4 mm. To obtain more data and also to check the effect of crack geometry and dimensions on the CTOA resistance curve, edge crack specimens with two different widths were used. The specimens were cut to produce an edge crack using a water-jet machine. Following the water jet cut, the notch was sharpened with a jewelers saw and fatigue loading was applied to produce a sharp crack. The specimens had the dimensions shown in Table 1. All the specimens were fatigued at the rate of 8 Hz using the fatigue load range shown in Table 1.

Table 1. Final dimensions of edge cracked specimens after fatigue loading.

Specimen	W (mm)	2L (mm)	Thickness t (mm)	Fatigue Load (kN)	No. of cycles	Final Crack Size, $2a_o$ (mm)
EC1	150	328	3.2	0.5-20.5	1923	48.50
EC2	75	354	3.2	0.5-10.5	4527	29.40
EC2	75	354	3.2	0.5-10.5	5010	29.52
EC2	75	354	3.2	0.5-10.5	5000	28.44

The fatigue-cracked specimens were loaded under stroke control at the rate of 0.001 mm/sec. As the crack began to grow, the loading was held constant at a certain length of crack extension and the digital image captured. The captured digital images were used to obtain the CTOA with crack extension for the specimens tested, using MATLAB. The stable crack extension, for the edge crack specimen with the large width, was close to 12.7 mm. For the edge crack specimen with a smaller width (75 mm), there was a similar length of stable crack extension of about 15 mm. For this reason, three edge crack specimens with the smaller width were tested to obtain more CTOA data. The data obtained from the CTOA measurement, using the acquired digital images from the fracture tests are shown in Figure 4, which also includes the data from center cracked specimens. Figure 5 shows images captured at different crack extension lengths using the edge crack specimen. Figure 6 shows the larger width edge crack specimen (EC1) and Figure 7 shows the edge crack specimen with the smaller width. Specimens of type EC1 are too wide to be placed directly into the hydraulic grips of the load-frame. Hence these specimens were bolted to a fixture which was gripped by the hydraulic grips.

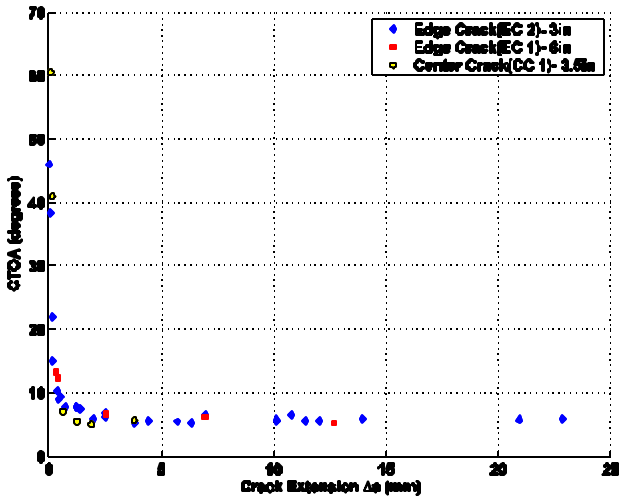

Figure 4. CTOA resistance curve for Al-2014-T6.

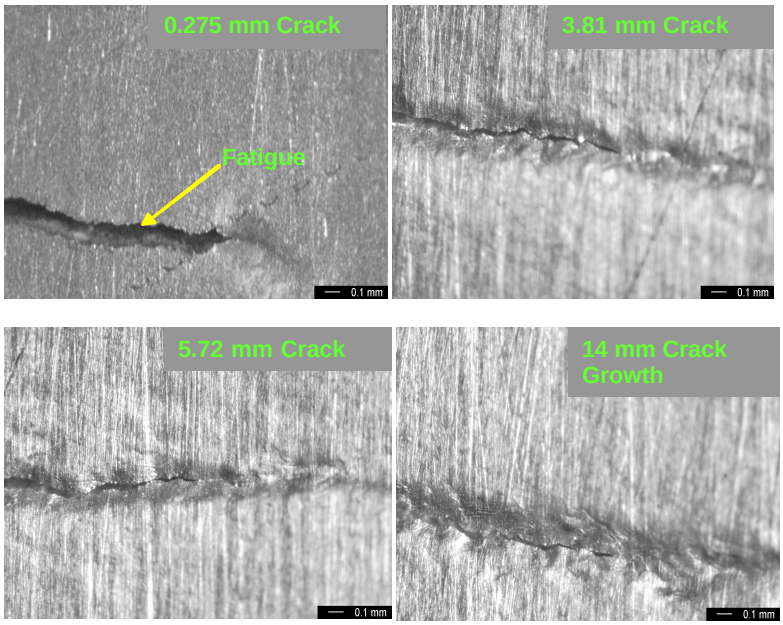

Figure 5. Crack tip region at various stages of crack growth for edge crack specimens EC2.

Figure 6. Edge cracked specimen EC1 with width W=150 mm.

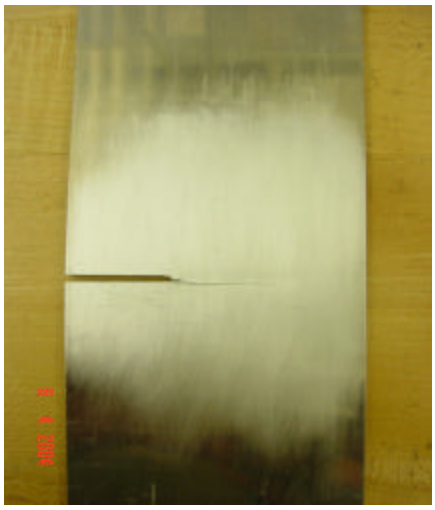

Figure 7. Edge cracked specimen EC2 with width W=75 mm.

2.1.3 AL-2014-T6 Tested at 100 and 200 ºC

The measurement of CTOA in Al-2014-T6 under 100 ^{o}C and 200 ^{o}C was conducted in a way similar to that for duplex steel. The data are presented in Figure 8.

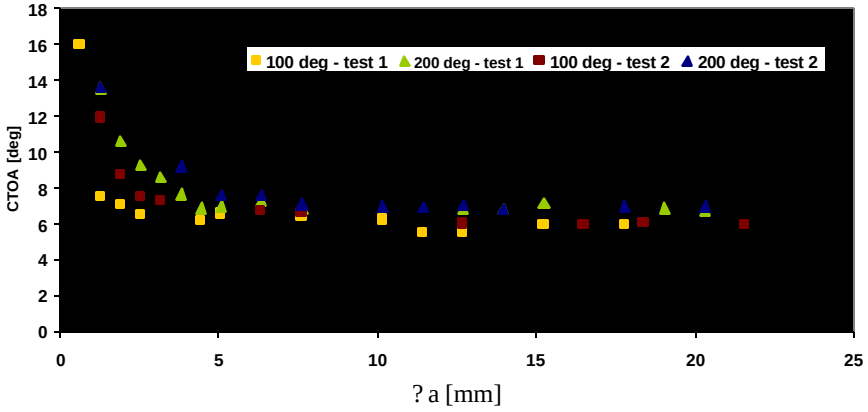

Figure 8. CTOA data for Al-2014-T6 at 100 and 200 ºC.

2.2 SIMULATION OF BURST OF THIN-WALLED CYLINDERS

2.2.1 CTOA Curve

2.2.1.1 Room Temperature CTOZ Curve

The CTOA data presented in Figure 9 for Al-2014-T6 at room temperature are used for the polynomial fit. The result is given as:

$$\begin{aligned} CTOA &= -0.2471(\Delta a)^3 + 2.601(\Delta a)^2 - 8.3(\Delta a) + 14.1, \qquad 0 \le \Delta a \le 2.45\, mm \\ CTOA &= 5.74, \qquad \Delta a > 2.45\, mm \end{aligned} \tag{1}$$

Figure 9 shows the CTOA curve and the data points.

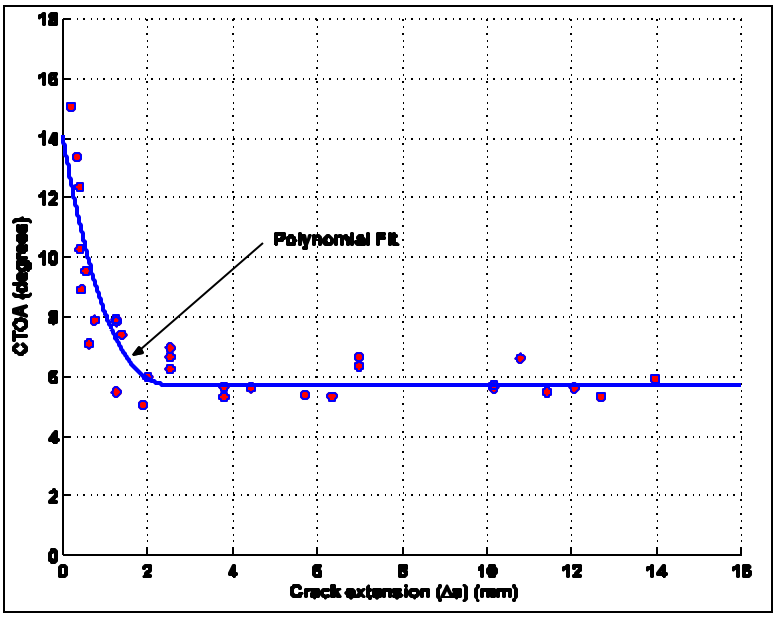

Figure 9. Polynomial fit of the CTOA data for Al-2014-T6 at room temperature.

2.2.1.2 Curve for 100 ºC

The CTOA curve for 100 ºC is described by the following:

$$CTOA = -0.0081 \cdot a^3 + 0.702 \cdot a^2 - 5.1322 \cdot a + 15.75°;\ 0 = < a = 4\ mm \qquad (2)$$

$$CTOA = 5.9348°;\ a > 4\ mm$$

The polynomial fit is shown in Figure 10.

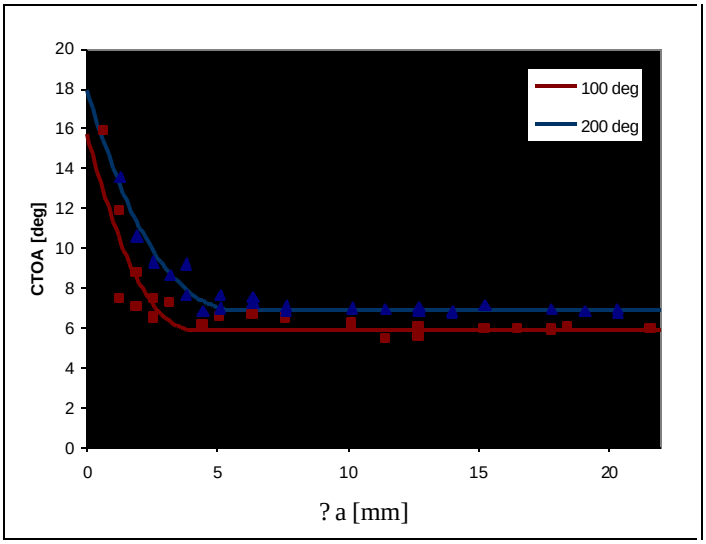

Figure 10. Polynomial fit of the CTOA data for Al-2014-T6 at 100 °C, and 200 °C.

2.2.1.3 CTOA Curve for 200 °C

The CTOA curve for 200 °C is described by the following:

$$CTOA = -0.0231 \cdot a^3 + 0.5845 \cdot a^2 - 4.5253 \cdot a + 17.95°;\ 0 = < a = 6\ mm \qquad (3)$$

$$CTOA = 6.8506°;\ a > 6\ mm$$

The polynomial fit is shown in Figure 10 along with the results for the 100 °C case.

2.3 MATERIAL PROPERTIES FOR AL-2014-T6

The stress-strain curve was obtained from tests conducted on dog-bone shaped specimens. Strain gauges were used to measure strains in the range from 0 to 5%. The large strains occurring during the test were determined using the laser extensometer. The laser measured strains were obtained from 0 to 16%. However, the measurements from a strain gauge are more accurate than the laser measurements for small strains. Figure 11 shows the stress-strain data for strain up to 5%. The Young's modulus for the material is found to be around 70 GPa. The material has a yield stress of about 425 MPa. Figure 12 shows the complete stress-strain curve obtained. Eight points along the stress-strain curve in the range from 425 MPa to 517 MPa corresponding to the plastic strains ranging from 0% to 12.5% were used for the elastic-plastic modeling in ABAQUS.

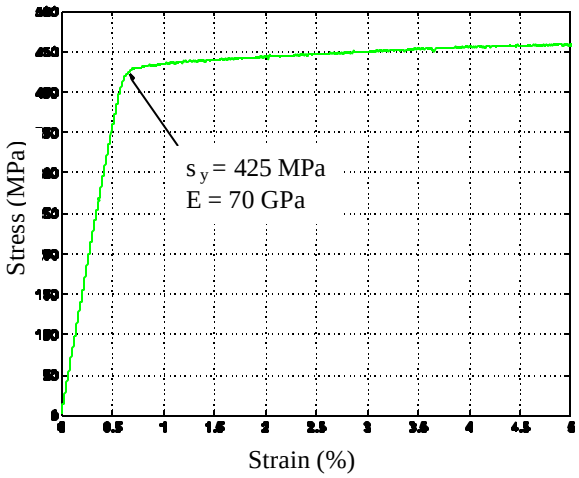

Figure 11. Stress-strain curve for Al-2014-T6 at room temperature.

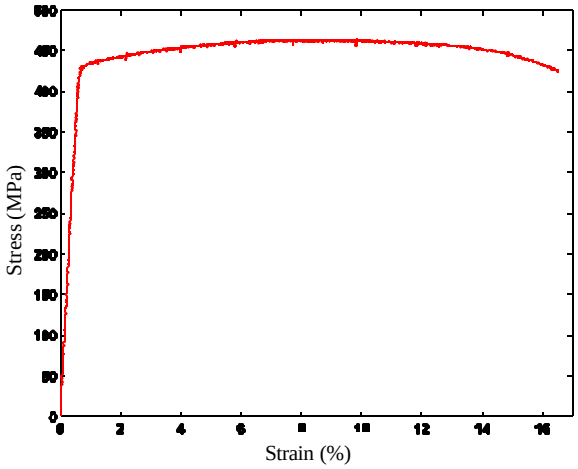

Figure 12. Full range of stress-strain curve for Al-2014-T6 at room temperature.

2.4 TEMPERATURE-DEPENDENT MECHANICAL PROPERTIES

Besides the CTOA curves, the mechanical properties of Al-2014-T6 in the temperature range of interest, were also needed. From Figure 13, which shows the Young's modulus of Al-2014-T6 as a function of temperature, it is noted that Young's modulus drops more quickly as temperature increases. Hence, the adopted approximation, which was taken from the Military Handbook of Materials 5 for Young's modulus in the temperature range of interest for Al-2014-T6 and is calculated by multiplying the room temperature value of Young's Modulus by the percentage indicated in the graph.

The yield stress as a function of temperature for Al-2014-T6 was found in the same manner as Young's modulus, by multiplying the room temperature yield stress by a certain percentage as plotted in the Military Mil-Handbook-5. Figure 14 is a reproduction showing this relationship as specified by Mil-Handbook-5 and it is specifically for Al-2014-T6. This was used to obtain the yield stresses for the high temperature stress strain curves and also the plastic portion of the curve as shown in Figure 15. This estimation of yield stress was then compared with the test results at high temperature from our lab, to validate the estimation. The graphical estimate for room temperature stress-strain and for stress-strain at 300 ºC was lower than the measured values

for the same cases. Thus, the measured data was used for the yield stress at that temperature in all of the finite element analyses. These stress-strain plots were then transferred as temperature dependant material data into the ABAQUS input file.

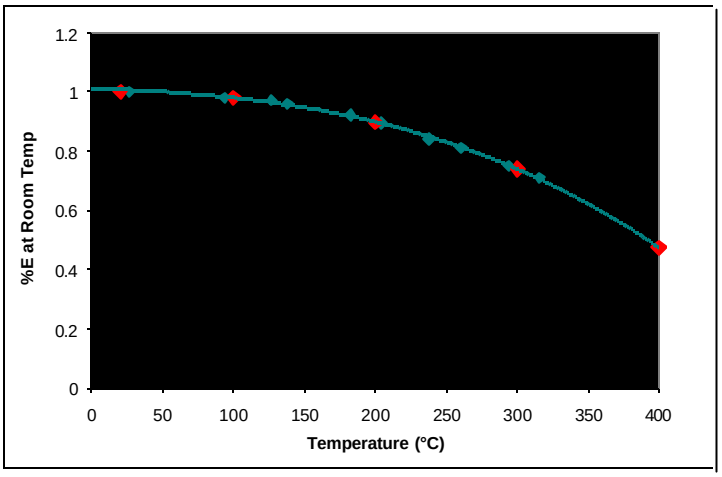

Figure 13. Young's modulus of Al-2014-T6 for elevated temperature (Mil-Handbook-5).

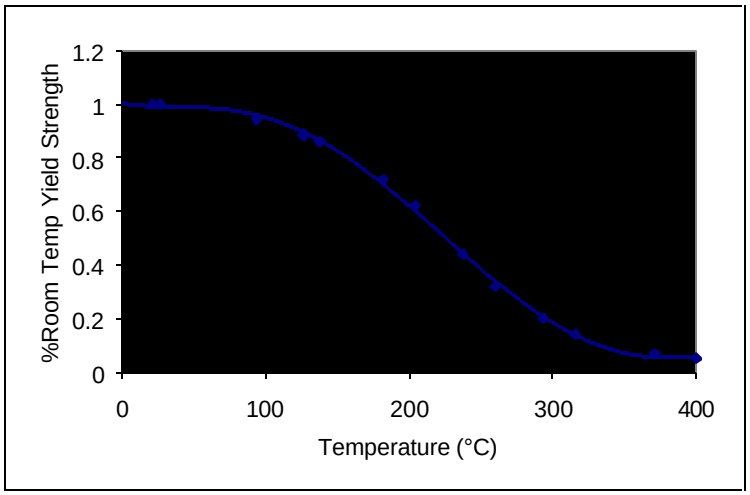

Figure 14. Yield stress of Al-2014-T6 vs. temperature (Mil-Handbook-5).

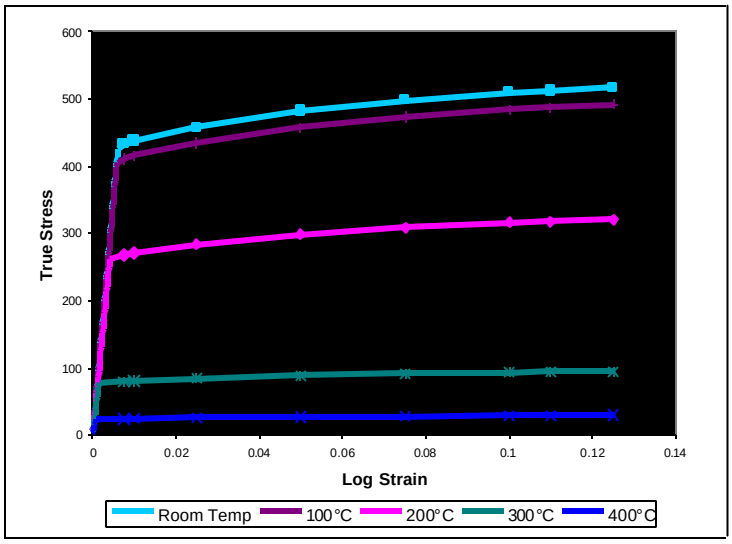

Figure 15. Constructed stress-strain curves for Al-2014-T6.

The data for the coefficient of thermal expansion were treated in a similar manner as they were reproduced from the Mil-Handbook-5 as well. Figure 16 represents the coefficients of thermal expansion specific to 20, 100, 200, 300, and 400 °C and the data was used for the ABAQUS input file's material property definition. The exact values used in the finite element analysis are listed in Table 2.

Table 2. Al-2014-T6 material properties for high temperature.

T (°C)	E_{LT} (GPa)	s^{YS} (MPa)	a (cm/cm-°C)
20	70	425.0	$22.29*10^{-6}$
100	68.536	403.8	$23.05*10^{-6}$
200	62.842	263.7	$23.81*10^{-6}$
300	51.693	111.5	$24.34*10^{-6}$
400	33.124	24.6	$24.65*10^{-6}$

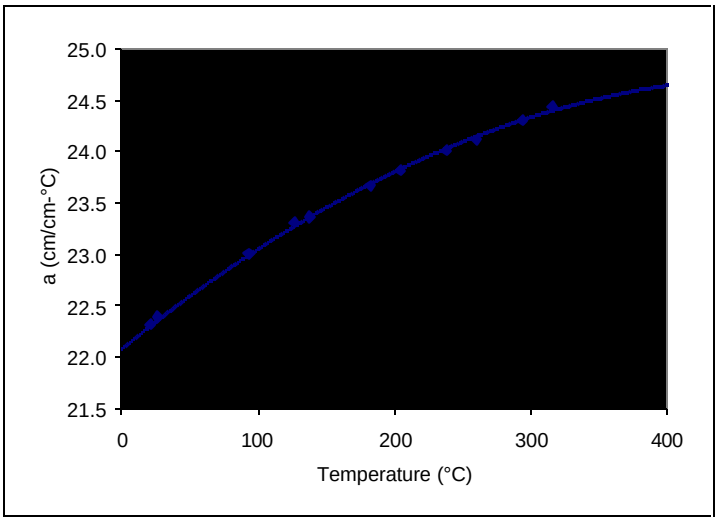

Figure 16. Coefficient of thermal expansion for Al-2014-T6.

2.5 SIMULATION OF BURST OF ALUMINUM CYLINDERS AT ROOM TEMPERATURE

The dimensions of the closed cylinder are listed in Table 3. Using the double symmetry and the loading condition of the model, one fourth of the full model was used in the simulation. Four noded shell elements (S4) were used to mesh the model. Four different lengths of the initial crack, namely 2a = 4, 8, 10, 14 cm were considered while maintaining the diameter of the cylinder for all the cases. The thickness of the cylinder was chosen to be the same as the Al-2014-T6 material used for the fracture tests, namely 3.2 mm. Figure 17 shows a representative mesh of the one-fourth cylinder model with the crack tip and the end cap indicated.

Table 3. Cylinder dimensions used in the study.

Cylinder	Diameter (D) (mm)	Length (L) (mm)	Crack Length (2a) (mm)	Thickness (mm)
1	254 (10 in)	722	40	3.2
2	254 (10 in)	742	80	3.2
3	254 (10 in)	752	100	3.2
4	254 (10 in)	772	140	3.2

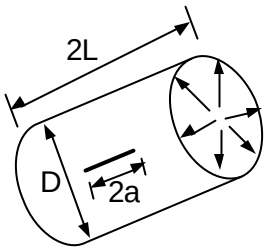

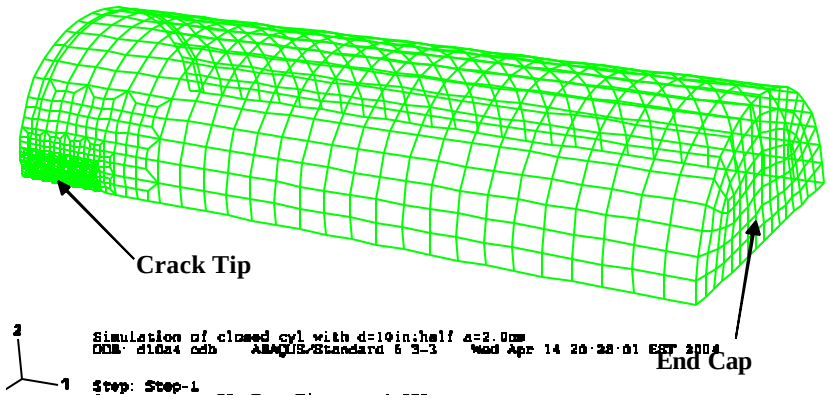

Figure 17. The mesh used in the analysis.

The critical CTOA criterion, which implicitly accounts for material non-linearity, is used as the appropriate parameter for modeling the crack growth of the cylinder. This section discusses the use of this parameter for the case of the cylinder shell subjected to internal pressure. As discussed in the previous section, the CTOA criterion is applied to Mode I fracture to determine the critical (or burst) pressure of the closed cylinder with internal pressure as the loading condition. The ABAQUS software is used to perform the finite element analysis (FEA) at every load step. Using the nodal displacements at every load step, the opening angle is computed and compared with the critical CTOA using a C++ program. After checking the opening angle, the C++ program computes the load, the location of the crack tip, the changed boundary conditions and writes the input file. This file is used to run the next load increment step with the ABAQUS FEA software. The above set of steps has to be repeated for every load increment made. A UNIX program is used for performing the ABAQUS FEA, extraction of nodal displacement data after the FEA, and running the C++ program in sequence for every load increment. If the opening angle is found to be more than the critical CTOA the pressure load is incrementally decreased until the opening angle matches the critical CTOA.

The material was modeled as elastic-plastic and the internal pressure was increased in small increments. The polynomial fit developed for the Al-2014-T6 material was used as the crack growth criterion. The internal pressure was increased for crack growth initially. After the critical

(or burst) pressure is reached, further crack extension at a steady state would be possible by reducing the internal pressure by small amounts after every increment of crack growth. Figure 18 shows the pressure P_{INIT} for crack growth to initiate, the maximum pressure P_{MAX} (or burst pressure) for the cylinder and the corresponding crack extension. Table 4 and summarize, respectively, the burst pressure predictions using the small and large deformation theories for the cylinders with the four different initial crack lengths. The burst pressure was also predicted using the large deformation theory for the cylinder with crack length 2a = 10 cm and 2a = 14 cm and the burst pressures were found to be smaller than the values predicted using small deformation. However the predictions obtained using the small deformation and large deformation theory were found to be close and within 3%.

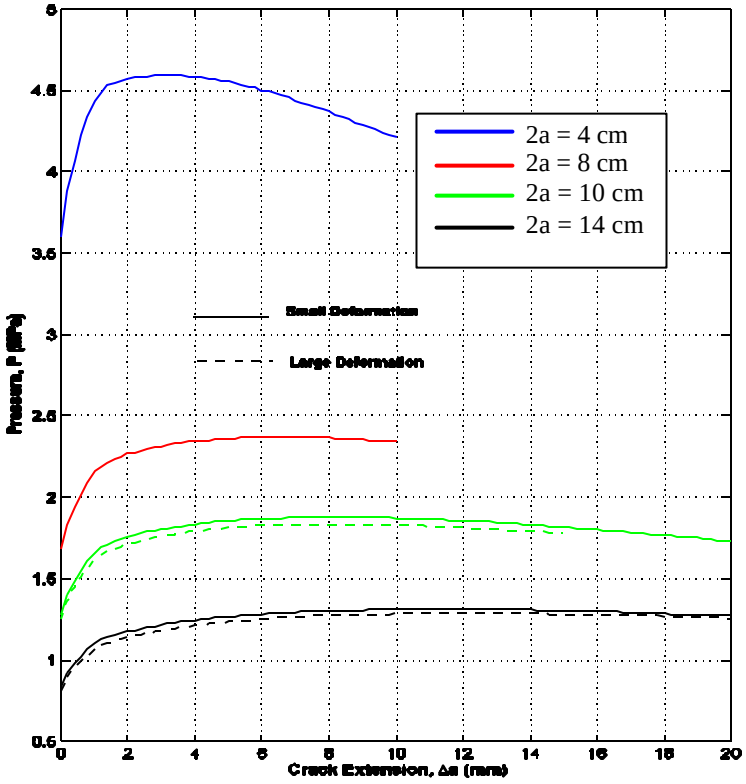

Figure 18. Crack history data for the four Al-2014-T6 cylinders.

Table 4. Burst pressure predictions for Al-2014-T6 cylinders with small deformation.

Cylinder	Diameter (mm)	Crack Length 2a (mm)	Thick t (mm)	P_{MAX} (MPa)	Crack Growth at Pmax ?a (mm)	P_{INIT} (MPa)
1	254 (10 in)	40	3.2	4.59	3.0	3.599
2	254 (10 in)	80	3.2	2.37	6.0	1.679
3	254 (10 in)	100	3.2	1.88	7.6	1.280
4	254 (10 in)	140	3.2	1.31	10.2	0.839

Table 5. Burst pressure predictions for Al-2014-T6 cylinders with large deformation.

Cylinder	Diameter (mm)	Crack Length 2a (mm)	Thick t (mm)	P_{MAX} (MPa)	Crack Growth at Pmax ?a (mm)	P_{INIT} (MPa)
3	254 (10 in)	100	3.2	1.83	7.6	1.253
4	254 (10 in)	140	3.2	1.29	11.4	0.816

2.6 A SENSITIVITY STUDY

In view of the scatter in CTOA data, it is desirable to evaluate the effect of the variation in the CTOA curve on the prediction of burst pressures. With this in mind, the aluminum CTOA curve was modified by lowering the initial section of the fit by ignoring a few of the initial nonlinear points. Figure 19 shows the modified curve and the original curve. Using the original and modified CTOA curves the simulation was performed and the results are shown in Figure 20. For comparison, the result obtained based on the constant CTOA of 5.74° is also included in the figure. It is evident that the modified CTOA curve gives results between that of the original CTOA curve and the constant CTOA assumption. There is a substantial deviation produced by the constant CTOA criterion.

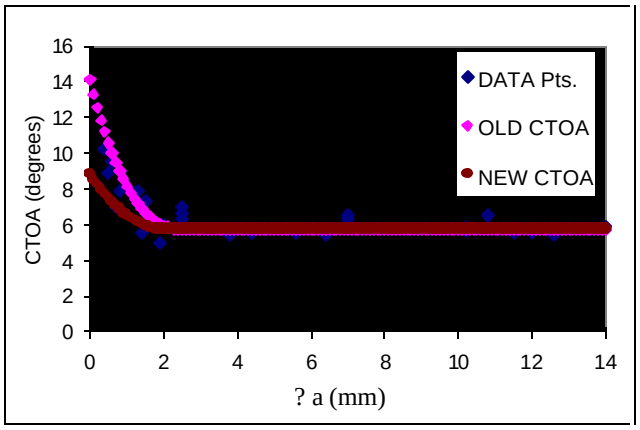

Figure 19. Modified (new) and original (old) CTOA curves for Aluminum 2014-T6.

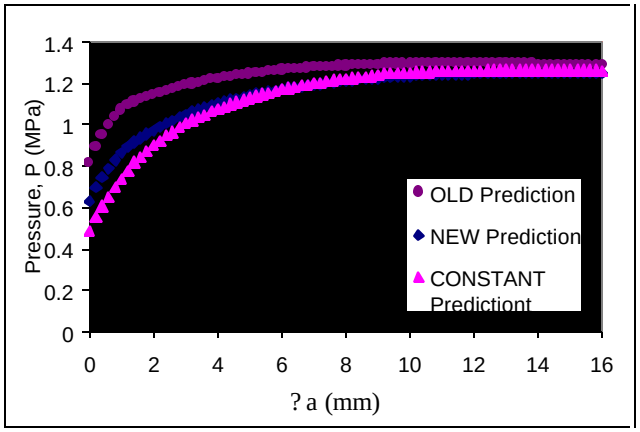

Figure 20. Simulation result with different CTOA curves.

2.7 SIMULATION OF BURST OF ALUMINUM CYLINDERS AT HIGH TEMPERATURE

The algorithm for determining the burst pressure of the cylinders with high temperatures is the same as that outlined for the predictions of the cylinders at room temperature. The major exception is that now the temperature of the body at each crack tip location must be used to specify which CTOA curve is needed to drive the crack propagation. This temperature tracking

was done easily due to the temperature fields being clearly predefined with exact dimensions while preparing the FEA models.

The high temperature was set at 400^{o}C and then transitioned in 1 cm/100 ^{o}C fields down to room temperature (20 ^{o}C). The correct CTOA curve was then selected based on the crack extension measurement (?a) as the crack propagated through the desired temperature fields. The remainder of the algorithm was discussed previously for the room temperature case.

The steps taken to apply the temperature in ABAQUS are as follows. A small pressure is applied initially to open the crack a small distance and then the temperature is increased to allow thermal strains to develop within the model. The first crack tip opening angle is then checked and the load is increased as needed to reach the critical opening angle. Finally, a small initial pressure was applied to prevent the crack faces from overlapping with the imaginary other half of the crack face. A comparison was done to determine if there was a difference in the burst pressure. This was accomplished by applying either an increase in the temperature or a small pressure.

The crack dimensions were the same as those used for the room temperature Aluminum cylinder. The crack was assumed to begin at the boundary between 200 ^{o}C and 100 ^{o}C with the crack tip node being at 100 ^{o}C for all crack lengths. The high temperature was set at 400^{o}C for all except for the 4 cm crack length cylinders. The highest temperature used for the 2a = 4 cm crack cylinder was 300 ^{o}C because there wasn't room to have a 400 ^{o}C zone and still begin the crack tip at the same location as the other three cylinders and retain the 1 cm transition zones.
The crack history results of these tests indicate that the heated zone increases the burst pressure of the cylinders as shown in Figure 21. Table 6 also lists the burst pressures and the percentage increased for each crack length from the room temperature predictions of burst pressure. This information is also shown in Figure 22.

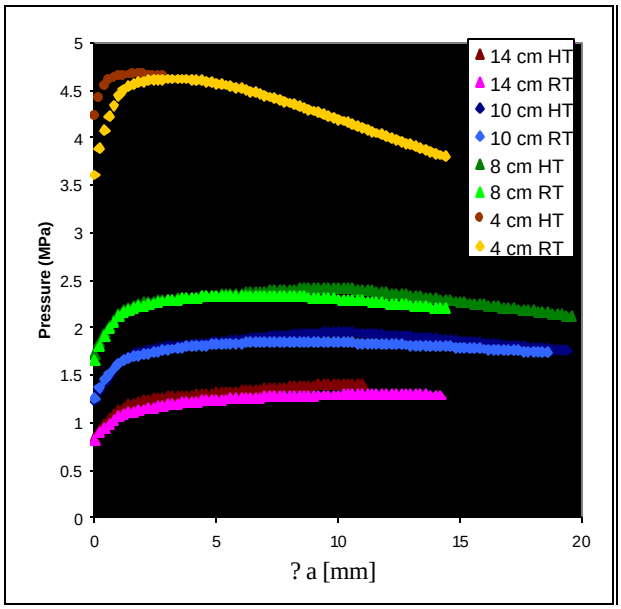

Figure 21. Crack history data for 10 cm diameter Al-2014-T6 cylinders tested at high temperatures.

Table 6. Variation in burst pressure by high temperature application.

2a (cm)	RT Pressure (MPa)	HT Pressure (MPa)	%change
4	4.620	4.664	0.96
8	2.341	2.425	3.58
10	1.848	1.953	5.66
14	1.296	1.412	9.00

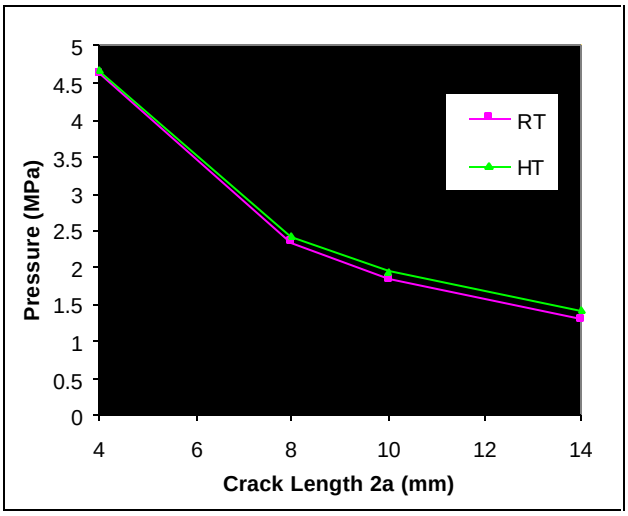

Figure 22. Burst pressure at different initial crack lengths increases with high temperatures.

A study was done for the initial condition of 2a = 4 cm to show how the burst pressure varied. This case was chosen due to its higher sensitivity to changes in the initial conditions. The premise of this study was to observe how the selection of the initial crack tip position, with respect to the high temperature fields, would vary the final outcome in terms of the burst pressure.

The study began by applying a high temperature field at the center of the crack in a circular region to resemble the heated zone of a localized heating source. The crack was then assumed to have come into existence at some initial length, 4 cm for the study, with the crack tip resting at the boundary of some high temperature region. The boundaries between reducing temperature transition fields were required to be 1 cm per 100 °C drop in temperature, from highest to lowest temperature.

The different cases considered in terms of the five temperature regions are shown in Figure 23.

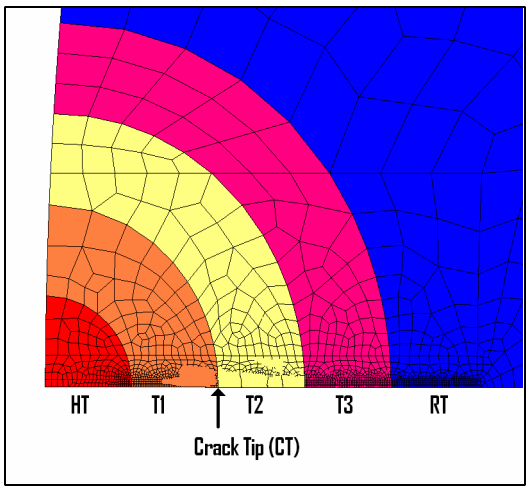

Case X: HT, T1, T2, T3, RT

Case 1: 20, 20, 20, 20, 20
Case 2: 100, 20, 20, 20, 20
Case 3: 200, 100, 20, 20, 20
Case 4: 300, 200, 100, 20, 20
Case 5: 400, 300, 200, 100, 20

Case 6: 100, 100, 20, 20, 20
Case 7: 100, 100, 100, 20, 20
Case 8: 200, 200, 100, 20, 20
Case 9: 300, 300, 200, 100, 20

Figure 23. High temperature fields used for the cylinder.

The overall outcome is that high temperature affects an increase in burst pressure for those cases where the crack tip is assumed to lie at 100 °C or less, as can be seen in Figure 24, and that it decreases it for those where the crack tip is located at 200 °C. Some explanations for this trend are in the material properties of Al-2014-T6 at elevated temperature. One is that the strength of Al-2014-T6 at 100 °C is 98% that of the room temperature material while the Crack Tip Opening Angle increases due to the rise in temperature (Figure 8). While holding temperature constant and increasing CTOA, an increase in required pressure to burst the cylinder is seen. The decrease in tensile properties is not great enough to make it reach the critical opening angle required by the increased CTOA curve. The second reason for the burst pressure increases is that the thermal expansion of the material acts to close the crack, increasing the pressure required to reach the critical CTOA. Therefore, the burst pressure must rise for these cases where the initial crack tip is assumed to lie at or below 100 °C. This rise in burst pressure can be seen in all the cases where the crack tip's temperature is at or less than 100 °C. This temperature increase, not being greater than 5% for any of the seven cases, indicates that this doesn't greatly affect the final burst pressure, as shown in Table 7. However, in the case of the tip assumed to be at the 200 °C point, the CTOA is increased, but the tensile material properties are now 90% of room temperature. This decrease allows the material to be compliant enough to reach the critical angle

at a lesser pressure than the cases with a smaller temperature loading. This is translated throughout the entire stable crack growth and results in a decreased burst pressure for those cases with crack tips at 200 °C. The change here is a more significant 12% drop in burst pressure for a crack developing through Case 5, for example. This can be thought of as effectively increasing the initial crack length by some ?a, which is a function of the temperature loading.

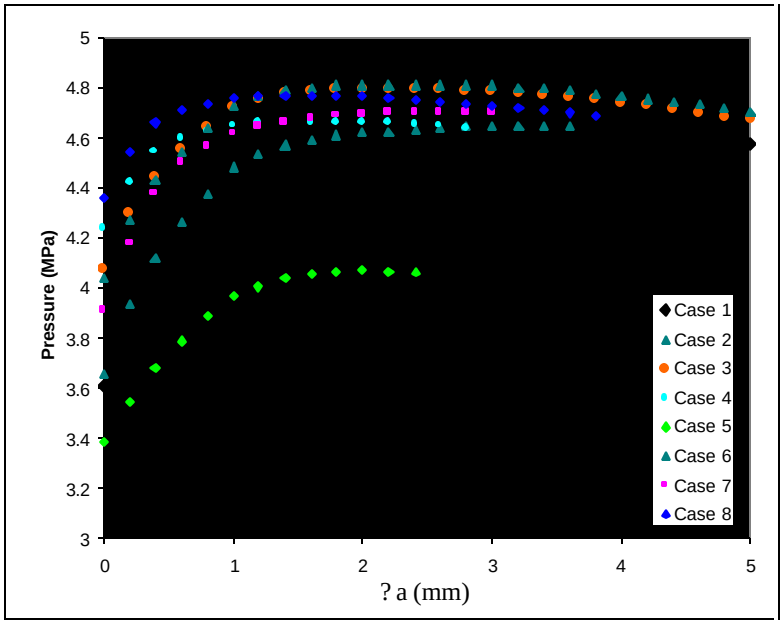

Figure 24. Al-2014-T6 cylinder with crack (2a=4 cm), pressure vs. crack extension.

Laboratory testing should be done to confirm this analysis and the simulation method employed to evaluate burst pressure prediction.

Table 7. Al-2014-T6 cylinder with 2a = 4 cm burst pressure CTOA fracture prediction due to variation in thermal loading.

CASE	P_{max} (MPa)	P_{init} (MPa)	% RT P_{max} Change
Initial Crack Tip at 20°C			
1: Room Temp	4.6195	3.609	0.0
2: 100, 20, 20, 20, 20 (ºC)	4.645	3.663	0.6
6: 100, 100, 20, 20, 20 (ºC)	4.813	4.045	4.2
3: 200, 100, 20, 20, 20 (ºC)	4.7955	4.077	3.8
Initial Crack Tip at 100°C			
7: 100, 100, 100, 20, 20 (ºC)	4.7016	3.909	1.8
8: 200, 200, 100, 20, 20 (ºC)	4.768	4.362	3.2
4: 300, 200, 100, 20, 20 (ºC)	4.664	4.239	1.0
Initial Crack Tip at 200°C			
5: 400, 300, 200, 100, 20 (ºC)	4.072	3.382	-11.9
9: 300, 300, 200, 100, 20 (ºC)		3.572	

3.0 CONCLUSIONS

For the four aluminum (Al-2014-T6) cylinders with a thickness of 3.175 mm, the predicted burst pressures under room temperature conditions obtained using the small deflection and large deformation theory were found to be close and within 3%. The sensitivity study showed that the effect of variation in the CTOA curve as a crack growth criterion on the burst pressure prediction was small. However the crack extension paths were different with different CTOA curves employed in the finite element nodal release simulation.

For the simulation of burst pressure of axially cracked pressurized aluminum cylinders at elevated temperature, the crack extension versus pressure plot indicated that the heated zone increased the burst pressure of the cylinders by almost ten percent. Laboratory testing should be conducted to investigate and confirm these analyses and simulation is good for burst pressure prediction of axially cracked cylinders subjected thermal and mechanical load.

4.0 BIBLIOGRAPHY

1. Peters, R. W. and Kuhn, P., 1957. Bursting Strength of Unstiffened Pressure Cylinder With Slits, NASA TN 3993.

2. Duffy, A. R., McClure, G. M., Eiber, R. J. and Maxey, W. A., 1965. Studies of Hydrostatic Test Levels And Defect Behavior, Symposium on Line Pipe Research, American Gas Association, New York.

3. Anderson, R. B. and Sullivan, T. L., 1966. Fracture Mechanics of Through-Cracked Cylindrical Pressure Vessels , NASA TN D-3252.

4. Hahn, G. T., Sarrate, M. and Rosenfield, A. R., 1969. "Criteria For Crack Extension In Cylindrical Pressure Vessels", *International Journal of Fracture Mechanics*, Vol. 5., pp. 187-210.

5. Kiefner, J. F., Maxey, W. A., Eiber, R. J. and Duffy, A. R., 1973. "Failure Stress Levels of Flaws In Pressurized Cylinders", in *Progress in Flaw Growth and Fracture Toughness Testing*, ASTM STP 536, pp. 461-481, American Society for Testing and Materials, Philadelphia.

6. Erdogan, F. and Ratwani, M., 1972. "Plasticity and The Crack Opening Displacement In Shells", *International Journal of Fracture Mechanics*, Vol. 8, pp. 413-426.

DISTRIBUTION LIST

DTIC/OCP 8725 John J. Kingman Rd, Suite 0944 Ft Belvoir, VA 22060-6218	1 cy
AFRL/VSIL Kirtland AFB, NM 87117-5776	2 cys
AFRL/VSIH Kirtland AFB, NM 87117-5776	1 cy
Ball Aerospace and Technologies Attn : Jennifer Rivera 2201 Buena Vista SE, Suite 100 Albuquerque, NM, 87106	1 cy
Official Record Copy AFRL/DELE/Robert Ulibarri	5 cys

This page is intentionally left blank.